ACS APPLIED BIO MATERIALS

www.acsabm.org Article

One-Dimensional Synergistic Core–Shell Nanozymes with Superior Peroxidase-like Activity for Ultrasensitive Colorimetric Detection of Blood Cholesterol

Hongzhen Peng, Jiaxing Zhang, Caixia Zeng, Chaoqun Zhou, Qingnuan Li,* Na Lu,* and Lihua Wang

Cite This: *ACS Appl. Bio Mater.* 2020, 3, 5111–5119 Read Online

ACCESS | Metrics & More | Article Recommendations | Supporting Information

ABSTRACT: In this paper, a simple and green strategy was proposed to fabricate one-dimensional core–shell Fe_3O_4@C/Ni nanocomposites. The rationally designed hybrid nanostructures notably exhibited an extremely excellent peroxidase-mimicking property, arising from the synergetic effects of Fe_3O_4, carbon, and Ni nanoparticles, along with the hollow and hierarchically porous nanostructures. Based upon the outstanding peroxidase-like activity and cholesterol oxidase cascade reaction, a label-free, ultrasensitive, and highly selective colorimetric assay for cholesterol determination has been developed. Under the optimized conditions, the colorimetric biosensor demonstrated a linear response to cholesterol ranging from 5 to 200 μM, with a relatively low detection limit of 0.17 μM. More importantly, cholesterol determination as low as 5 μM could be directly distinguished with the naked eye. In addition, we successfully determined the total cholesterol content in human serum samples with satisfactory accuracy and good precision. The Fe_3O_4@C/Ni nanocatalyst-based colorimetric biosensor provides great potential in point-of-care testing in disease diagnosis.

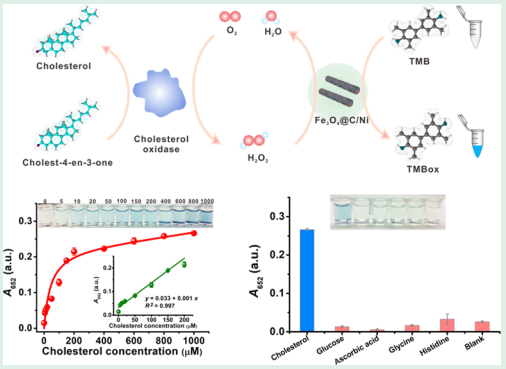

KEYWORDS: *one-dimensional, nanozyme, peroxidase-like, ultrasensitive, colorimetric detection, cholesterol*

INTRODUCTION

Blood cholesterol is a waxy, fat-like substance existing in blood, fat, and cells, which plays an important role in making hormones, digesting fatty foods, and formatting cell membranes. However, a normal level of blood cholesterol from 2.9 to 6.0 mM is essential in maintaining good health. Suggested evidence indicates that high cholesterol put us at risk for heart disease and stroke but has no signs or symptoms. Until now, various techniques, such as chromatography,[1] enzyme-linked immunosorbent assay (ELISA),[2] electrochemiluminescence,[3] fluorescence,[4−6] and electrochemistry,[7−9] have been used for cholesterol detection. However, to our knowledge, they are still challenging because of laborious experimental procedures, complicated pretreatment, and expensive instrumentation. Therefore, it is of great significance to develop a simple, cost-effective, and reliable method of monitoring cholesterol levels to prevent cardiovascular disease.

Rapid advances in nanoscience and nanotechnology[10−18] enable the creation of nanomaterials with unique properties and superior features, which have been widely applied in many research areas, including biosensing,[19−21] biomedicine,[22−24] catalysis,[25−28] and energy storage.[29−32] A typical example among them is the nanozyme, which possesses intrinsic enzyme-mimicking characteristics as a new generation of artificial enzymes. Significant research efforts have been made to explore nanozymes because of the unparalleled features of easy preparation, low cost, and high stability. Until now, nanozymes with different enzyme-like activities have been reported, for example, peroxidase mimics, oxidase mimics, catalase mimics, multienzyme mimics, and so forth. In particular, nanozymes with peroxidase-like activity, such as ferromagnetic nanoparticles (NPs),[33,34] gold NPs,[35] carbon-based nanomaterials,[36] and nanocomposites,[37,38] have been extensively explored for their broad applications in the detection of glucose,[39] nucleic acids,[40] proteins,[41,42] and even microorganisms.[43] Despite the progress, the intrinsic structural constraints from zero- or two-dimensional nanomaterials, such as NP aggregation caused by noncovalent interactions[44] and nonspecific absorptions,[45] still limit their applications. Given the remarkable benefits of high surface area, efficient electron transfer, and good biocompatibility, one-dimensional (1D) nanomaterials have emerged as a promising candidate to construct biosensors, which have been utilized in the detection of DNA, cancer markers, viruses, cells, and even tissues.[46−50]

Received: May 19, 2020
Accepted: July 7, 2020
Published: July 7, 2020

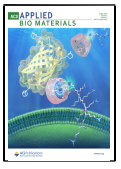

https://dx.doi.org/10.1021/acsabm.0c00588
ACS Appl. Bio Mater. 2020, 3, 5111–5119

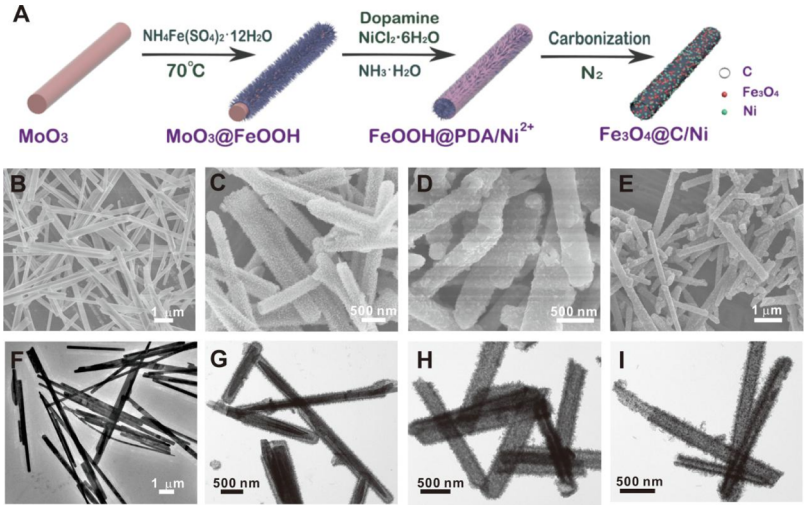

Figure 1. (A) Scheme of Fe_3O_4@C/Ni nanocomposite synthesis. (B–I) SEM and TEM images of (B,F) MoO_3 nanorods, (C,G) MoO_3@FeOOH nanocomposites, (D,H) FeOOH@PDA/Ni^{2+} nanocomposites, and (E,I) Fe_3O_4@C/Ni nanocomposites.

However, few studies have been reported for cholesterol determination by using 1D nanomaterials as peroxidase mimics.

To fill up this gap, we proposed a simple, facile, and green synthetic procedure to fabricate 1D core–shell Fe_3O_4@C/Ni nanocomposites, which exhibited superior peroxidase-mimicking activities because of the synergetic effects of Fe_3O_4, carbon, and Ni NPs. Coupling the outstanding peroxidase-mimicking activity and cholesterol oxidase cascade reactions, a simple, label-free, ultrasensitive, and highly selective colorimetric assay for cholesterol detection has been developed. More importantly, cholesterol determination could be directly identified by the naked eye. Furthermore, the total cholesterol in the human serum sample was successfully determined.

MATERIALS AND METHODS

Materials. Ammonium molybdate tetrahydrate ($(NH_4)_6Mo_7O_{24}\cdot 4H_2O$), sodium borohydride ($NaBH_4$), nickel chloride hexahydrate ($NiCl_2\cdot 6H_2O$), ammonium hydroxide (28–30%), ammonium ferric sulfate dodecahydrate ($NH_4Fe(SO_4)_2\cdot 12H_2O$), 3,3′,5,5′-tetramethylbenzidine (TMB), and 30% hydrogen peroxide (H_2O_2) were from Sinopharm Chemical Reagent Co., Ltd. (Shanghai, China). Dopamine hydrochloride was purchased from Thermo Fisher Scientific (China) Co., Ltd. Cholesterol oxidase was obtained from Sigma-Aldrich Co. (St. Louis, MO, USA). Cholesterol was obtained from Sangon Biotech Co., Ltd. (Shanghai, China). Double-distilled water (ddH_2O) was employed in all aqueous solutions.

Apparatus. Morphology measurements were performed using a JEOL-4800 scanning electron microscope (JEOL, Japan) and a JEM-1011 transmission electron microscope (JEOL, Japan) operating at 200 kV, respectively. UV–vis absorption measurements were recorded by using a UV-2450 spectrophotometer (Shimadzu, Japan).

Preparation of Fe_3O_4@C/Ni Nanocomposites. Typically, the template of MoO_3 nanorods was first prepared through a hydrothermal method as previously reported.[51] Then, 1 g of $(NH_4)_6Mo_7O_{24}\cdot 4H_2O$ was dissolved in a 10% HNO_3 solution. After complete dissolution, the mixture was fed into a Teflon-lined stainless steel autoclave and reacted for 20 h at 180 °C. Next, 0.091 M ammonium ferric sulfate solution was introduced dropwise into the dispersed MoO_3 nanorods (10% ethanol) with mechanical agitation. After reaction for 4 h at 70 °C, MoO_3@FeOOH nanocomposites were obtained. Subsequently, 2 mL of the ammonia aqueous solution was mixed with the MoO_3@FeOOH nanocomposites under stirring. Afterward, 30 mg of dopamine and 75.2 mg of $NiCl_2\cdot 6H_2O$ were introduced to the above solution for reaction for 16 h to produce FeOOH@PDA/Ni^{2+}. Finally, the final product Fe_3O_4@C/Ni nanocomposites were obtained by carbonization of FeOOH@PDA/Ni^{2+} at 500 °C for 5 h.

Peroxidase-like Activity. The peroxidase-like activity of the as-prepared Fe_3O_4@C/Ni nanocomposite was determined as follows. Briefly, the dispersed Fe_3O_4@C/Ni nanocatalyst (100 μg mL^{-1}) was added into the 0.2 M acetate buffer at pH 4.0 with TMB (0.2 mM) and H_2O_2 (0.1 mM), and then, the mixed solution reacted for 10 min at 50 °C. After magnetic separation, the reacted solution without Fe_3O_4@C/Ni was measured using a UV–vis spectrophotometer.

Colorimetric Detection. For H_2O_2 detection, 20 μg mL^{-1} Fe_3O_4@C/Ni nanocatalyst, 0.05 mM TMB, and different concentrations of H_2O_2 (1, 5, 10, 20, 50, 100, 200, 500, 1000, and 2000 μM) were added into the 0.2 M acetate buffer solution at pH 4.0. After 10 min incubation at 50 °C, the absorbance spectra were recorded immediately.

For cholesterol detection, the experimental procedures were conducted as follows. Typically, 10 μL of cholesterol oxidase (1 mg mL^{-1}) and 10 μL of varying concentrations of cholesterol (5, 10, 20, 50, 100, 200, 500, and 1000 μM) were mixed with 80 μL of phosphate-buffered saline (PBS, pH 7.4). Then, the mixed solution was incubated at 37 °C for 30 min. Thereafter, the above solution was injected into 385 μL of 0.2 M acetate buffer at pH 4.0 containing 2 μL of the Fe_3O_4@C/Ni nanocatalyst (20 μg mL^{-1}) and 12.5 μL of TMB (0.05 mM). After incubation for 10 min at 50 °C, the nanocatalyst was separated by applying an external magnetic field. Finally, the absorption spectrum measurement of the resulting reaction solution was performed.

RESULTS AND DISCUSSION

Fabrication of Fe_3O_4@C/Ni Nanocomposites. Figure 1A illustrates the programmable synthetic process of the Fe_3O_4@C/Ni nanocomposites. Initially, MoO_3 nanorods were fabricated through green hydrothermal synthesis.[56] The scanning electron microscopy (SEM) image in Figure 1B showed a highly uniform 1D smooth tubular morphology, which was 170–300 nm in diameter with a length of several micrometers. From the transmission electron microscopy (TEM) image (Figure 1F), it was clearly seen that the MoO_3 nanorods exhibited a solid architecture without obvious porosity. Then, the FeOOH shell was loaded on the surface of MoO_3 templates to form coaxial MoO_3@FeOOH nanostructures via hydrolysis of Fe^{3+} at 70 °C. After coating, a bristlelike morphology with an increased diameter of 230–380 nm was observed from the SEM image (Figure 1C). Furthermore, the

https://dx.doi.org/10.1021/acsabm.0c00588
ACS Appl. Bio Mater. 2020, 3, 5111–5119

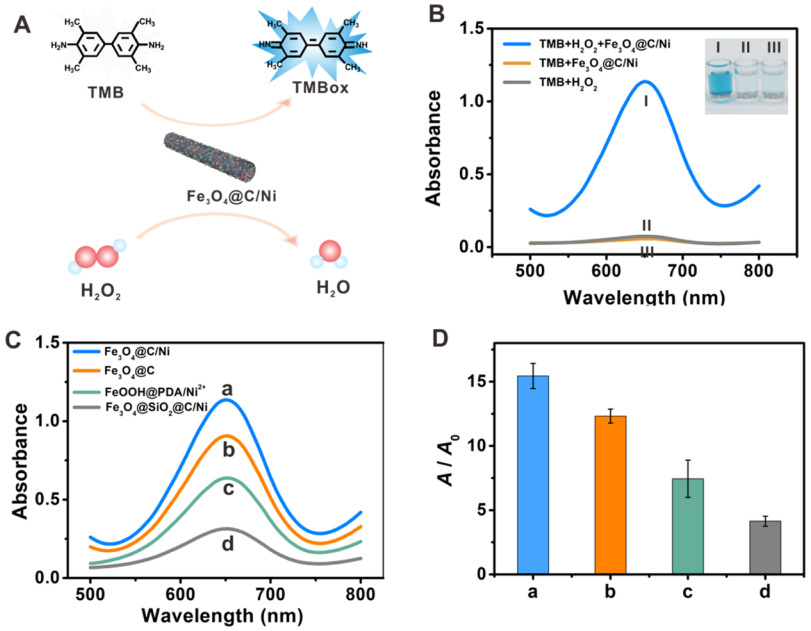

Figure 2. (A,B) Peroxidase-mimicking activity of Fe_3O_4@C/Ni nanocomposites. (A) Schematic representation of the Fe_3O_4@C/Ni nanocomposites showing peroxidase-like activity. (B) UV−vis spectra and photographs of different reaction systems, (I) TMB + H_2O_2 + Fe_3O_4@C/Ni nanocomposites, (II) TMB + Fe_3O_4@C/Ni nanocomposites, and (III) TMB + H_2O_2. (C,D) UV−vis spectra (C) and comparison (D) of the catalytic oxidation toward TMB by different nanocatalysts, (a) Fe_3O_4@C/Ni, (b) Fe_3O_4@C, (c) FeOOH@PDA/Ni^{2+}, and (d) Fe_3O_4@SiO_2@C/Ni nanocomposites. The amount of nanocatalyst, TMB, and H_2O_2 was 100 μg mL^{-1}, 0.1 mM, and 0.2 mM, respectively. The reaction systems were performed in a 0.2 M HAc−NaAc buffer at pH 4.0 at 50 °C for 10 min of incubation.

TEM image in Figure 1G demonstrated that the MoO_3@FeOOH nanocomposite was an obvious core−shell nanostructure, in which burrlike FeOOH nanostructures were uniformly distributed onto the surface of the MoO_3 nanorod. Subsequently, FeOOH@PDA-Ni^{2+} nanocomposites were fabricated through a simple one-step procedure, in which polydopamine (PDA) and Ni^{2+} were coated together on the surface, and MoO_3 templates were removed by wet etching of ammonia in the meantime. From Figure 1D,H, it could be seen that the obtained FeOOH@PDA/Ni^{2+} nanocomposites showed a rough surface morphology with a thick coated layer and a hollow tubular structure, suggesting successful deposition of the amorphous PDA/Ni^{2+} layer and total removal of MoO_3 templates. Finally, the Fe_3O_4@C/Ni nanocomposites were produced by carbonizing FeOOH@PDA/Ni^{2+} under a nitrogen atmosphere. After carbonization, the prepared Fe_3O_4@C/Ni nanocomposites still retained geometrically 1D tubular morphologies with numerous uniform and well-dispersed Ni NPs (Figure 1E,I). In addition, X-ray diffraction (XRD) was employed to study the crystallographic properties of the Fe_3O_4@C/Ni nanocomposites (Figure S1). The six characteristic peaks at 2θ corresponded to the standard diffraction planes of Fe_3O_4,[39] confirming the successful change of FeOOH to Fe_3O_4.

To study the electronic state between elements of the Fe_3O_4@C/Ni nanocomposites, X-ray photoelectron spectroscopy (XPS) was performed. As anticipated, it clearly showed the prominent peaks corresponding to the main elements of C, N, O, Fe, and Ni (Figure S2A). In the high-resolution scan, two main peaks of Fe appeared at 711.2 and 725.0 eV (Figure S2B), which were assigned to Fe $2p_{3/2}$ and Fe $2p_{1/2}$, respectively.[52] The deconvoluted Fe $2p_{3/2}$ XPS spectrum has two peaks located at the binding energies of 710.0 and 711.4 eV, which could be ascribed to Fe^{3+} and Fe^{2+}, respectively (Figure S2C),[51] indicating the existence of Fe_3O_4. Furthermore, two peaks of Ni 2p were in accordance with Ni at the zero-valence state (Figure S2D),[53] confirming the formation of Ni NPs. Additionally, the N 1s spectrum could be deconvoluted into two peaks, which corresponded to C═N and C−N-type bonds, respectively (Figure S2E).[54]

In addition, the magnetic property of the Fe_3O_4@C/Ni nanocomposites was studied via a vibrating sample magnetometer. The magnetization hysteresis loop exhibited a sigmoid-shaped curve at room temperature, with little hysteresis and remanence (Figure S2F). Moreover, the magnetic curve showed a saturation value of 13.4 emu g^{-1}, indicating a quick separation of the nanocomposites from the solution within a few seconds under a magnetic field. Moreover, nitrogen adsorption and desorption isotherms revealed that the Brunauer−Emmett−Teller surface area of the Fe_3O_4@C/Ni nanocomposites was 77.1 m^2 g^{-1}, possessing a mean pore diameter of ∼11 nm (Figure S3), indicating the mesoporous properties.

Enzyme-Mimicking Property of Fe_3O_4@C/Ni. To evaluate the enzyme-mimicking property of the Fe_3O_4@C/Ni nanocomposites, a representative catalytic reaction of oxidizing the chromogenic substrate TMB in the presence of H_2O_2 was used (Figure 2A). As shown in Figure 2B, the colorless TMB solution rapidly changed into dark blue with the introduction of the Fe_3O_4@C/Ni nanocomposites, where a characteristic absorbance at 652 nm appeared, similar to that of horseradish peroxidase (HRP). In contrast, in the presence of either Fe_3O_4@C/Ni or H_2O_2 alone, it showed almost no visible color change or characteristic absorption peak at 652 nm under the same conditions. These results successfully confirmed an intrinsic peroxidase-mimicking activity of the Fe_3O_4@C/Ni nanocomposites.

https://dx.doi.org/10.1021/acsabm.0c00588
ACS Appl. Bio Mater. 2020, 3, 5111−5119

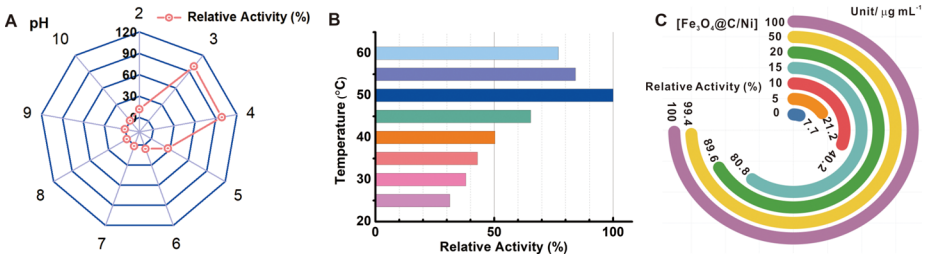

Figure 3. Dependence of the peroxidase-like activity of the Fe_3O_4@C/Ni nanocomposites on pH (A), temperature (B), and nanocatalyst concentration (C).

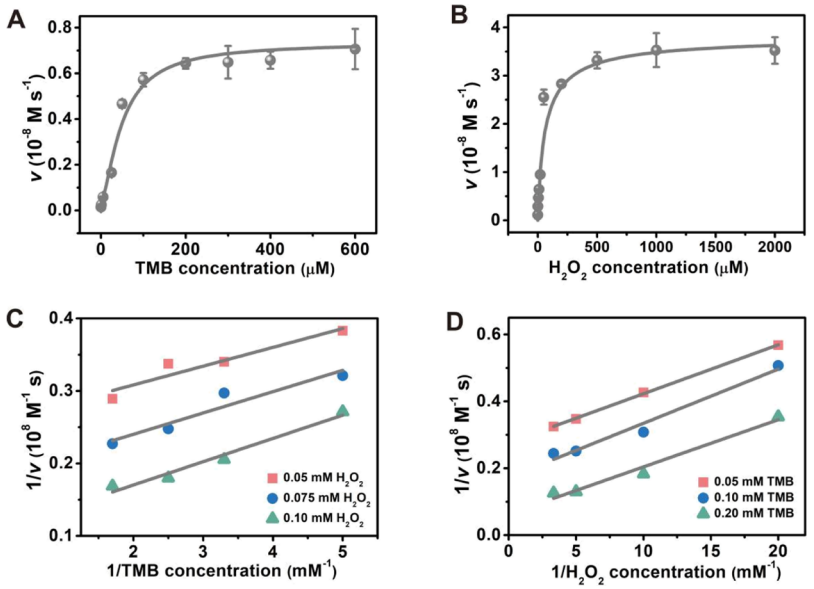

Figure 4. Steady-state kinetic assays of the Fe_3O_4@C/Ni nanocomposites. (A) Velocity of the reaction changes by varying TMB concentrations while keeping the concentration of H_2O_2 at 0.05 mM. (B) Velocity of the reaction changes by varying H_2O_2 concentrations while keeping the concentration of TMB at 0.05 mM. (C) Lineweaver–Burk plots obtained against TMB when H_2O_2 was fixed at three levels (0.05, 0.075, and 0.10 mM). (D) Lineweaver–Burk plots obtained against H_2O_2 when TMB was fixed at three levels (0.05, 0.10, and 0.20 mM).

Moreover, the catalytic activity of Fe_3O_4@C/Ni nanocomposites was compared with that of other iron oxide-based 1D nanomaterials. As shown in Figure 2C, the as-prepared Fe_3O_4@C/Ni nanocomposites showed the highest peroxidase-like activity with a maximum absorbance at 652 nm. To better evaluate the catalytic effects, we defined the relative signal change A/A_0, where A represents the absorbance at 652 nm in the presence of nanocatalysts and A_0 corresponds to the absorbance at 652 nm of the blank sample. Interestingly, it was found that the Fe_3O_4@C/Ni nanocomposites produced a relative signal change as high as ~16-fold, which was much larger than that of the Fe_3O_4@C nanowire (NW) (~12-fold) (Figure 2D), suggesting that anchored Ni NPs enhanced the catalytic efficiency of Fe_3O_4@C/Ni nanocomposites.[55] Moreover, either the reaction intermediate FeOOH@PDA/Ni^{2+} or Fe_3O_4@SiO_2@C/Ni nanocomposites gave an even smaller catalytic response. The results demonstrated that Fe_3O_4 and carbon play the crucial roles in the enzyme-mimicking activity, while the addition of the SiO_2 shell goes against the peroxidase-like activity. We speculated that the outstanding peroxidase-mimicking catalytic ability arose from the synergetic effects of Fe_3O_4, carbon, and Ni NPs, along with the hollow, aligned, and hierarchically porous architectures, which could speed up the electron transfer and produce more active radical species on the surface of the nanomaterial.[56] Eventually, it resulted in a significant enhancement of peroxidase-mimicking ability of the Fe_3O_4@C/Ni nanozyme and acceleration of the electron transfer in the biosensing process.

Similar to other nanomaterial-based enzyme mimics, the enzyme-mimicking property of the Fe_3O_4@C/Ni nanocomposites was also dependent on pH, temperature, and concentration of the nanocatalyst. As shown in Figure 3A,B, the catalytic activity of the Fe_3O_4@C/Ni nanocomposites was investigated in different pH buffers from 2.0 to 10.0 and at temperatures from 25 to 55 °C. Notably, either the absorbance (Figure 3A) or color change (Figure S4) showed a maximum change in the pH range from 3.0 to 4.0. In view of the leaching of the iron ions from Fe_3O_4 NPs at a low pH (⩽3.0),[57] we selected pH 4.0 as the optimal reaction medium. In addition, the catalytic activity increased with the temperature and reached the maximum at 55 °C (Figure 3B). Figure 3C shows that the catalytic oxidation reaction toward TMB was also dependent on the concentration of the nanocatalyst. The absorbance gradually increased with the concentration, followed by a gentle trend above 50 μg mL^{-1}. Thus, the 0.2 M acetate buffer at pH 4.0, a temperature of 55 °C, and 50 μg mL^{-1} nanocatalyst were selected as the optimal conditions.

Kinetic Analysis and the Catalytic Mechanism. To gain a deep understanding of the catalytic mechanism, enzyme kinetic models and methods were employed to investigate the

https://dx.doi.org/10.1021/acsabm.0c00588
ACS Appl. Bio Mater. 2020, 3, 5111–5119

catalytic activity of the Fe_3O_4@C/Ni nanocomposites. Steady-state reaction assays were carried out by varying the concentration of one substrate while keeping the concentration of the other constant. As shown in Figure 4A,B, the reciprocal of the reaction rate versus the concentration of the substrate was plotted, with TMB and H_2O_2 as substrates within a certain range, which followed the typical Michaelis–Menten curve. Then, the Lineweaver–Burk double reciprocal plots were fitted against one substrate when the other was fixed at three different levels (Figure 4C,D). By comparing with the natural enzyme HRP and other nanocatalysts, apparent kinetic parameters such as Michaelis–Menten constant (K_m) and maximal initial velocity (V_{max}) were determined according to the Lineweaver–Burk equation. As is well known, K_m is considered as an indicator of enzyme affinity toward the substrate. A low K_m indicates high affinity to the substrate and vice versa. As illustrated in Table 1, when H_2O_2 was used as a substrate, the Michaelis–Menten constant value of the as-prepared Fe_3O_4@C/Ni was 62 times lower than that of HRP. In comparison with Fe_3O_4 NP and Fe_3O_4@C NW, Fe_3O_4@C/Ni also exhibited an ~2610-fold and 3-fold decrease in the K_m value, respectively. Moreover, Fe_3O_4@C/Ni showed higher or comparable affinity toward TMB in comparison with HRP or other nanocatalysts. The results demonstrated strong affinity of Fe_3O_4@C/Ni toward both H_2O_2 and TMB, demonstrating an ultrasensitive detection potential in biomedical applications. Furthermore, the slopes of the fitted lines in Figure 4C,D were parallel, revealing a ping-pong mechanism.

Table 1. Comparison of the Kinetic Parameters with Natural Enzyme and Other Nanocatalysts

catalyst	substrate	K_m (mM)	V_{max} (10^{-8} M s^{-1})
Fe_3O_4@C/Ni NW	TMB	0.10	3.90
	H_2O_2	0.059	3.62
HRP[33]	TMB	0.434	10
	H_2O_2	3.7	8.71
Fe_3O_4 NP[33]	TMB	0.098	3.44
	H_2O_2	154	9.78
Fe_3O_4@C NW[42]	TMB	0.20	1.34
	H_2O_2	0.23	2.41

Colorimetric Detection of H_2O_2 and Cholesterol. H_2O_2 acts as an important signaling molecule in cells and is involved in many biological processes. On the basis of the excellent enzyme-mimicking properties of the Fe_3O_4@C/Ni nanocatalyst, a simple and label-free colorimetric assay for H_2O_2 detection was developed. Figure 5A shows that the characteristic absorbance at 652 nm continuously increased with the increasing concentration of H_2O_2. Meanwhile, the color change from colorless to deep blue toward the oxidation of TMB was also observed, with a visual limit of detection (LOD) at 10 μM. Moreover, a linear response ranging from 1 to 50 μM (R^2 = 0.993) was observed, with a detection limit of 48 nM, considering the 4δ of a target-blank sample (Figure 5B).

The simple, rapid, and accurate monitoring of the cholesterol level is very pivotal for disease control and prevention. Therefore, a label-free, ultrasensitive, and highly selective strategy to determine cholesterol is desirable for point-of-care diagnosis. Herein, inspired by the peroxidase-like activity of the Fe_3O_4@C/Ni nanocomposite, we developed a facile colorimetric cholesterol assay by incorporating cholesterol oxidase and the TMB chromogenic reaction (Figure 6A). In a typical procedure, cholesterol oxidase catalyzes the oxidation of cholesterol into cholest-en-3-one in a PBS buffer (pH 7.4). Meanwhile, oxygen is converted to H_2O_2. Subsequently, the Fe_3O_4@C/Ni nanocatalyst catalyzes the substrate TMB by in situ produced H_2O_2. As illustrated in Figure 6B, varying concentrations of cholesterol were quantitatively determined through the absorbance changes at 652 nm. The absorbance increased with the increasing concentration of cholesterol, which generated a color variation by visual identification as low as 5 μM. The inset in Figure 6B shows that the absorbance exhibited a linear correction to the concentration of cholesterol (R^2 = 0.997) from 5 to 200 μM with a relatively low detection limit of 0.17 μM. By comparison with the nanomaterial-based biosensors for H_2O_2 and cholesterol, our proposed biosensor demonstrated excellent analytical performance, which was more sensitive than or comparable to that of previously reported nanomaterial-based bioassays (Table 2).

To examine the selectivity of the proposed assay, common small molecules, such as glucose, ascorbic acid, glycine, and histidine, were selected as possible interferents. It was found that the absorbance was maintained as low as the background level even if the concentration of the interferent was 20 times as high as that of cholesterol (Figure 6C). Meanwhile, from the inset in Figure 6C, the color difference could be easily visualized with the naked eye.

To explore the practical applications of our proposed biosensor, the determination of the total cholesterol content was performed in 50-fold diluted human serum samples. After pretreating the serum samples as per previous reports, the samples were determined, and recovery experiments were analyzed in Table 3. This revealed that the average recoveries of three spiked human serum samples for cholesterol ranged from 93 to 104% as well as a good precision of the relative

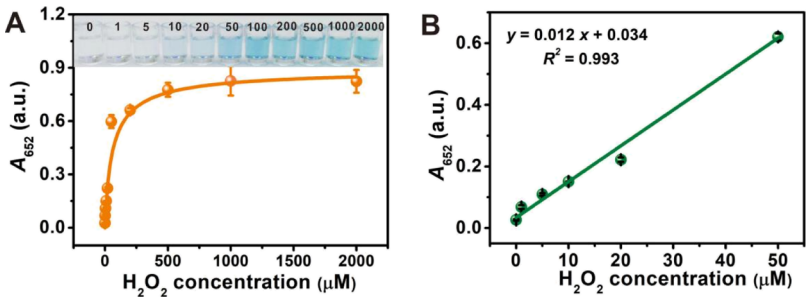

Figure 5. (A) Plot of the absorbance change at 652 nm vs the concentration of H_2O_2 from 1 to 2000 μM. The inset photograph shows the colored TMB solution with varying concentrations of H_2O_2. (B) Linear calibration curve for H_2O_2 determination.

https://dx.doi.org/10.1021/acsabm.0c00588
ACS Appl. Bio Mater. 2020, 3, 5111–5119

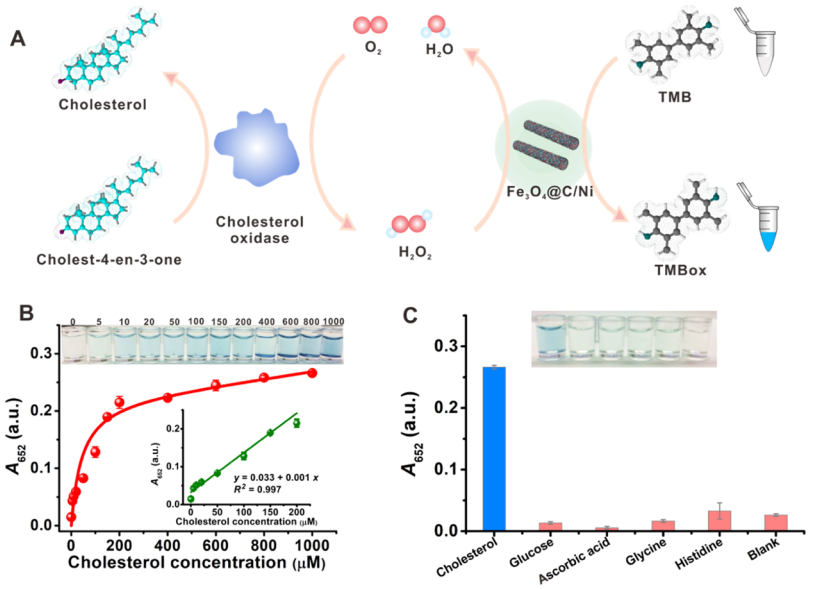

Figure 6. (A) Schematic representation of the colorimetric assay for cholesterol determination based upon Fe_3O_4@C/Ni catalysis. (B) Plot of the absorbance change at 652 nm vs the concentration of cholesterol from 5 to 1000 μM. The inset photograph shows the colored TMB solution with varying concentrations of cholesterol. The inset shows the linear calibration curve of cholesterol concentration. (C) Selectivity analysis for cholesterol detection. The inset photograph shows the corresponding visual color change. The concentrations were as follows: 1 mM cholesterol, 20 mM glucose, 20 mM ascorbic acid, 20 mM glycine, 20 mM histidine, and the blank sample. The error bars represent the standard deviations of three measurements.

Table 2. Comparison of Various Nanomaterial-Based Biosensors for H_2O_2 and Cholesterol[a]

target	detection techniques	nanomaterial	linear range	LOD	refs
H_2O_2	EC	Fe_3O_4@Ag nanocomposites	0.5−20 μM	0.16 μM	58
H_2O_2	colorimetry	FePt−Au hybrid NPs	20−700 μM	12.33 μM	59
H_2O_2	FL	MnO_2 nanosheets−FAM complex	1−200 μM	0.33 μM	5
H_2O_2	SPR	bio@AgNP nanohybrids	30−1000 μM	73.50 μM	6
	FL		30−1000 μM	93.50 μM	
H_2O_2	EC	AuPt/ZIF-8-rGO	100 nM-18 mM	19 nM	7
H_2O_2	EC	Fe−Nx-doped graphitic nanocages	1−5000 μM	0.53 μM	60
H_2O_2	colorimetry	Fe_3O_4@C/Ni nanotubes	1−50 μM	48 nM	this work
cholesterol	CL	Cu nanoclusters	0.05−10 mM	1.5 μM	61
cholesterol	colorimetry	boron nitride nanosheet@CuS nanohybrids	10−100 μM	2.9 μM	62
cholesterol	FL	MnO_2 nanosheets−FAM complex	1−300 μM	0.33 μM	5
cholesterol	SPR	bio@AgNP nanohybrids	1−40 μM	8.16 μM	6
	FL		1−40 μM	5.50 μM	
cholesterol	colorimetry	MXene−Ti_3C_2/CuS nanocomposites	10−100 μM	1.9 μM	63
cholesterol	colorimetry	Mo, S codoped carbon quantum dots	10−600 μM	7 μM	64
cholesterol	colorimetry	Fe_3O_4@C/Ni nanotubes	5−200 μM	0.17 μM	this work

[a]EC: electrochemistry. FL: fluorescence. CL: chemiluminescence.

Table 3. Determination Results of Cholesterol in Human Serum Samples via Our Proposed Method

sample	original amount (μM)	added (μM)	found (μM)	recovery (%)	RSD (%)
1	106	0	102	96	3.16
		4	108	98	3.56
		10	112	94	2.91
		20	130	103	1.41
2	98	0	94	95	4.16
		4	98	93	4.22
		10	112	104	3.37
		20	114	96	1.98

standard deviation (RSD) of less than 5%. It suggested that the Fe_3O_4@C/Ni-based colorimetric assay demonstrated wide potential applications in cholesterol determination in real serum samples.

By comparison with other reported cholesterol biosensors, our bioassay possesses several significant advantages. First of all, the proposed cholesterol biosensor is a label-free colorimetric assay, not requiring any complicated biomolecular labeling or sophisticated instrumentation. Second, the as-prepared Fe_3O_4@C/Ni nanocatalyst shows high affinity toward the substrate and an enhanced catalytic activity, thus enabling an ultrasensitive detection of blood cholesterol. In addition, for the bioassay, the cholesterol level could be directly determined with the naked eye, which was very easy and helpful for daily uses. Therefore, this simple, cost-effective,

https://dx.doi.org/10.1021/acsabm.0c00588
ACS Appl. Bio Mater. 2020, 3, 5111−5119

and easy-to-operate method for cholesterol determination is attractive for point-of-care testing.

CONCLUSIONS

In summary, we fabricated 1D core−shell Fe_3O_4@C/Ni nanocomposites with low cost, good water dispersion, magnetic nature, and good biocompatibility via a simple and green solvothermal synthesis. The rationally designed Fe_3O_4@C/Ni nanocomposites showed a superior peroxidase-like activity and high affinity toward two substrates, TMB and H_2O_2, benefiting from the synergetic effect of Fe_3O_4, carbon, and Ni nanozymes as well as the hierarchically porous and hollow nanostructures. On the basis of the catalytic activity, coupling with the cholesterol oxidase reaction, we developed a label-free, cost-effective, and reliable colorimetric assay for cholesterol determination. The proposed biosensor presented ultrahigh sensitivity as well as good selectivity toward cholesterol determination. Moreover, the cholesterol level could be monitored by the naked eye, without any special instrumentation, which was appropriate for point-of-care service. Moreover, the total cholesterol content in human serum samples has been determined by our proposed sensor with satisfactory results. We envision that this colorimetric strategy holds promising potential in medical diagnostics and biocatalysis.

ASSOCIATED CONTENT

Supporting Information

The Supporting Information is available free of charge at https://pubs.acs.org/doi/10.1021/acsabm.0c00588.

XRD spectrum, XPS spectra, magnetization curve, and nitrogen adsorption−desorption isotherms of the Fe_3O_4@C/Ni nanocomposites and photograph of TMB solutions in varying pH in the presence of the Fe_3O_4@C/Ni nanocomposites (PDF)

AUTHOR INFORMATION

Corresponding Authors

Qingnuan Li − *Shanghai Institute of Applied Physics, Chinese Academy of Sciences, Shanghai 201800, China*; Email: liqingnuan@sinap.ac.cn

Na Lu − *School of Materials Engineering, Shanghai University of Engineering Science, Shanghai 201620, China*; orcid.org/0000-0001-5771-247X; Email: nlu2014@163.com

Authors

Hongzhen Peng − *Division of Physical Biology and Bioimaging Center, CAS Key Laboratory of Interfacial Physics and Technology, Shanghai Institute of Applied Physics, Chinese Academy of Sciences, University of Chinese Academy of Sciences, Shanghai 201800, China; Shanghai Synchrotron Radiation Facility, Zhangjiang Laboratory, Shanghai Advanced Research Institute, Chinese Academy of Sciences, Shanghai 201210, China*

Jiaxing Zhang − *School of Materials Engineering, Shanghai University of Engineering Science, Shanghai 201620, China*

Caixia Zeng − *School of Materials Engineering, Shanghai University of Engineering Science, Shanghai 201620, China*

Chaoqun Zhou − *Pennsylvania State University, State College, Pennsylvania 16803, United States*

Lihua Wang − *Shanghai Synchrotron Radiation Facility, Zhangjiang Laboratory, Shanghai Advanced Research Institute, Chinese Academy of Sciences, Shanghai 201210, China; Shanghai Key Laboratory of Green Chemistry and Chemical Processes, School of Chemistry and Molecular Engineering, East China Normal University, Shanghai 200241, China*; orcid.org/0000-0002-6198-7561

Complete contact information is available at: https://pubs.acs.org/10.1021/acsabm.0c00588

Notes

The authors declare no competing financial interest.

ACKNOWLEDGMENTS

This work was financially supported by the National Key Research and Development Program (2016YFA0201200), the National Natural Science Fund of China (81974317), and the Talent Program of Shanghai University of Engineering Science.

REFERENCES

(1) Zhao, M.; Bergaentzlé, M.; Flieller, A.; Marchioni, E. Development and Validation of an Ultra-High Performance Liquid Chromatography-High Resolution Mass Spectrometry Method for Simultaneous Quantification of Cyanogenic Glycosides and Secoisolariciresinol Diglucoside in Flaxseed. *J. Chromatogr. A* **2019**, *1601*, 214−223.

(2) Chalupova, L.; Zakovska, A.; Adamcova, K. Development of a Novel Enzyme-linked Immunosorbent Assay (ELISA) for Measurement of Serum CTRP1 A Pilot Study: Measurement of Serum CTRP1 in Healthy Donors and Patients with Metabolic Syndrome. *Clin. Biochem.* **2013**, *46*, 73−78.

(3) Yang, D.-P.; Guo, W.; Cai, Z.; Chen, Y.; He, X.; Huang, C.; Zhuang, J.; Jia, N. Highly Sensitive Electrochemiluminescence Biosensor for Cholesterol Detection Based on AgNPs-BSA-MnO_2 Nanosheets with Superior Biocompatibility and Synergistic Catalytic Activity. *Sensor. Actuator. B Chem.* **2018**, *260*, 642−649.

(4) Lu, N.; Wen, Y.; Liu, G.; Ding, L.; Zeng, C.; Aldalbahi, A.; Khan, M. N.; Periyasami, G.; Rahaman, M.; Alrohaili, A.; Shi, J.; Song, S.; Wang, L.; Zhang, M. Multifunctional Yolk-Shell Nanostructure as A Superquencher for Fluorescent Analysis of Potassium Ion Using Guanine-Rich Oligonucleotides. *ACS Appl. Mater. Interfaces* **2017**, *9*, 30406−30413.

(5) Han, T.; Zhu, S.; Wang, S.; Wang, B.; Zhang, X.; Wang, G. Fluorometric Methods for Determination of H_2O_2, Glucose and Cholesterol by Using MnO_2 Nanosheets Modified with 5-Carboxyfluorescein. *Microchim. Acta* **2019**, *186*, 269.

(6) Xu, H. V.; Zhao, Y.; Tan, Y. N. Nanodot-Directed Formation of Plasmonic-Fluorescent Nanohybrids toward Dual Optical Detection of Glucose and Cholesterol via Hydrogen Peroxide Sensing. *ACS Appl. Mater. Interfaces* **2019**, *11*, 27233−27242.

(7) Zhang, T.; Xing, Y.; Song, Y.; Gu, Y.; Yan, X.; Lu, N.; Liu, H.; Xu, Z.; Xu, H.; Zhang, Z.; Yang, M. AuPt/MOF-Graphene: A Synergistic Catalyst with Surprisingly High Peroxidase-Like Activity and Its Application for H_2O_2 Detection. *Anal. Chem.* **2019**, *91*, 10589−10595.

(8) Gao, A.; Lu, N.; Wang, Y.; Dai, P.; Li, T.; Gao, X.; Wang, Y.; Fan, C. Enhanced Sensing of Nucleic Acids with Silicon Nanowire Field Effect Transistor Biosensors. *Nano Lett.* **2012**, *12*, 5262−5268.

(9) Su, S.; Han, X.; Lu, Z.; Liu, W.; Zhu, D.; Chao, J.; Fan, C.; Wang, L.; Song, S.; Weng, L.; Wang, L. Facile Synthesis of a MoS_2-Prussian Blue Nanocube Nanohybrid-Based Electrochemical Sensing Platform for Hydrogen Peroxide and Carcinoembryonic Antigen Detection. *ACS Appl. Mater. Interfaces* **2017**, *9*, 12773−12781.

(10) Chen, J.; Badioli, M.; Alonso-González, P.; Thongrattanasiri, S.; Huth, F.; Osmond, J.; Spasenović, M.; Centeno, A.; Pesquera, A.; Godignon, P.; Zurutuza Elorza, A.; Camara, N.; de Abajo, F. J. G.; Hillenbrand, R.; Koppens, F. H. L. Optical Nano-imaging of Gate-tunable Graphene Plasmons. *Nature* **2012**, *487*, 77−81.

(11) Wang, Y.; Xu, J.; Wang, Y.; Chen, H. Emerging Chirality in Nanoscience. *Chem. Soc. Rev.* **2013**, *42*, 2930−2962.
(12) Lu, N.; Pei, H.; Ge, Z.; Simmons, C. R.; Yan, H.; Fan, C. Charge Transport within a Three-Dimensional DNA Nanostructure Framework. *J. Am. Chem. Soc.* **2012**, *134*, 13148−13151.
(13) Yan, Y.; Shi, X. R.; Miao, M.; He, T.; Dong, Z. H.; Zhan, K.; Yang, J. H.; Zhao, B.; Xia, B. Y. Bio-Inspired Design of Hierarchical FeP Nanostructure Arrays for the Hydrogen Evolution Reaction. *Nano Res.* **2018**, *11*, 3537−3547.
(14) He, W.; Guo, X.; Zheng, J.; Xu, J.; Hayat, T.; Alharbi, N. S.; Zhang, M. Structural Evolution and Compositional Modulation of ZIF-8-Derived Hybrids Comprised of Metallic Ni Nanoparticles and Silica as Interlayer. *Inorg. Chem.* **2019**, *58*, 7255−7266.
(15) Zheng, J.; Zhang, M.; Miao, T.; Yang, J.; Xu, J.; Alharbi, N. S.; Wakeel, M. Anchoring Nickel Nanoparticles on Three-Dimensionally Macro-/Mesoporous Titanium Dioxide with a Carbon Layer from Polydopamine Using Polymethylmethacrylate Microspheres as Sacrificial Templates. *Mater. Chem. Front.* **2019**, *3*, 224−232.
(16) Hu, Q.; Li, H.; Wang, L.; Gu, H.; Fan, C. DNA Nanotechnology-Enabled Drug Delivery Systems. *Chem. Rev.* **2019**, *119*, 6459−6506.
(17) Lu, N.; Wang, L.; Lv, M.; Tang, Z.; Fan, C. Graphene-Based Nanomaterials in Biosystems. *Nano Res.* **2019**, *12*, 247−264.
(18) Zhang, M.; Ding, L.; Zheng, J.; Liu, L.; Alsulami, H.; Kutbi, M. A.; Xu, J. Surface Modification of Carbon Fibers with Hydrophilic Fe_3O_4 Nanoparticles for Nickel-Based Multifunctional Composites. *Appl. Surf. Sci.* **2020**, *509*, 145348.
(19) Labib, M.; Sargent, E. H.; Kelley, S. O. Electrochemical Methods for the Analysis of Clinically Relevant Biomolecules. *Chem. Rev.* **2016**, *116*, 9001−9090.
(20) Tian, R.; Ji, J.; Zhou, Y.; Du, Y.; Bian, X.; Zhu, F.; Liu, G.; Deng, S.; Wan, Y.; Yan, J. Terminal-Conjugated Non-Aggregated Constraints of Gold Nanoparticles on Lateral Flow Strips for Mobile Phone Readouts of Enrofloxacin. *Biosens. Bioelectron.* **2020**, *160*, 112218.
(21) Zhu, D.; Liu, W.; Zhao, D.; Hao, Q.; Li, J.; Huang, J.; Shi, J.; Chao, J.; Su, S.; Wang, L. Label-Free Electrochemical Sensing Platform for MicroRNA-21 Detection Using Thionine and Gold Nanoparticles Co-Functionalized MoS_2 Nanosheet. *ACS Appl. Mater. Interfaces* **2017**, *9*, 35597−35603.
(22) Blanco, E.; Shen, H.; Ferrari, M. Principles of Nanoparticle Design for Overcoming Biological Barriers to Drug Delivery. *Nat. Biotechnol.* **2015**, *33*, 941−951.
(23) Mura, S.; Nicolas, J.; Couvreur, P. Stimuli-Responsive Nanocarriers for Drug Delivery. *Nat. Mater.* **2013**, *12*, 991−1003.
(24) Kouser, R.; Vashist, A.; Zafaryab, M.; Rizvi, M. A.; Ahmad, S. pH-Responsive Biocompatible Nanocomposite Hydrogels for Therapeutic Drug Delivery. *ACS Appl. Bio Mater.* **2018**, *1*, 1810−1822.
(25) Shi, X.-R.; Zhang, Y.; Zong, S.; Gu, W.; Ma, P.; Lu, N. Interaction of Ethylene with Ir-n (n=1-10): From Bare Clusters to gamma-Al_2O_3-Supported Nanoparticles. *Nanomaterials* **2019**, *9*, 331.
(26) Gao, D.; Arán-Ais, R. M.; Jeon, H. S.; Roldan Cuenya, B. Rational Catalyst and Electrolyte Design for CO_2 Electroreduction towards Multicarbon Products. *Nat. Catal.* **2019**, *2*, 198−210.
(27) Zheng, Y.; Vasileff, A.; Zhou, X.; Jiao, Y.; Jaroniec, M.; Qiao, S.-Z. Understanding the Roadmap for Electrochemical Reduction of CO_2 to Multi-Carbon Oxygenates and Hydrocarbons on Copper-Based Catalysts. *J. Am. Chem. Soc.* **2019**, *141*, 7646−7659.
(28) Chen, P.; Zhao, G.; Shi, X.-R.; Zhu, J.; Ding, J.; Lu, Y. Nano-Intermetallic $InNi_3C_{0.5}$ Compound Discovered as a Superior Catalyst for CO_2 Reutilization. *iScience* **2019**, *17*, 315−324.
(29) Larcher, D.; Tarascon, J.-M. Towards Greener and More Sustainable Batteries for Electrical Energy Storage. *Nat. Chem.* **2015**, *7*, 19−29.
(30) Dunn, B.; Kamath, H.; Tarascon, J.-M. Electrical Energy Storage for the Grid: A Battery of Choices. *Science* **2011**, *334*, 928−935.
(31) Guo, Y.; Cao, Y.; Chen, Z.; Li, R.; Gong, W.; Yang, W.; Zhang, Q.; Wang, H. Fluorinated Metal-Organic Framework as Bifunctional Filler toward Highly Improving Output Performance of Triboelectric Nanogenerators. *Nano Energy* **2020**, *70*, 104517.
(32) Zhang, S.; Zhang, X.; Shi, X.; Zhou, F.; Wang, R.; Li, X. Facile Fabrication of Ultrafine Nickel-iridium Alloy Nanoparticles/Graphene Hybrid with Enhanced Mass Activity and Stability for Overall Water Splitting. *J. Energy Chem.* **2020**, *49*, 166−173.
(33) Gao, L.; Zhuang, J.; Nie, L.; Zhang, J.; Zhang, Y.; Gu, N.; Wang, T.; Feng, J.; Yang, D.; Perrett, S.; Yan, X. Intrinsic Peroxidase-Like Activity of Ferromagnetic Nanoparticles. *Nat. Nanotechnol.* **2007**, *2*, 577−583.
(34) Zeng, C.; Lu, N.; Wen, Y.; Liu, G.; Zhang, R.; Zhang, J.; Wang, F.; Liu, X.; Li, Q.; Tang, Z.; Zhang, M. Engineering Nanozymes Using DNA for Catalytic Regulation. *ACS Appl. Mater. Interfaces* **2019**, *11*, 1790−1799.
(35) Hizir, M. S.; Top, M.; Balcioglu, M.; Rana, M.; Robertson, N. M.; Shen, F.; Sheng, J.; Yigit, M. V. Multiplexed Activity of perAuxidase: DNA-Capped AuNPs Act as Adjustable Peroxidase. *Anal. Chem.* **2016**, *88*, 600−605.
(36) Song, Y.; Qu, K.; Zhao, C.; Ren, J.; Qu, X. Graphene Oxide: Intrinsic Peroxidase Catalytic Activity and Its Application to Glucose Detection. *Adv. Mater.* **2010**, *22*, 2206−2210.
(37) Zhang, J.; Lu, N.; Peng, H.; Li, J.; Yan, R.; Shi, X.; Ma, P.; Lv, M.; Wang, L.; Tang, Z.; Zhang, M. Multi-Triggered and Enzyme-Mimicking Graphene Oxide/polyvinyl Alcohol/G-Quartet Supramolecular Hydrogels. *Nanoscale* **2020**, *12*, 5186−5195.
(38) Tan, B.; Zhao, H.; Wu, W.; Liu, X.; Zhang, Y.; Quan, X. Fe_3O_4-AuNPs Anchored 2D Metal-Organic Framework Nanosheets with DNA Regulated Switchable Peroxidase-Like Activity. *Nanoscale* **2017**, *9*, 18699−18710.
(39) Lu, N.; Zhang, M.; Ding, L.; Zheng, J.; Zeng, C.; Wen, Y.; Liu, G.; Aldalbahi, A.; Shi, J.; Song, S.; Zuo, X.; Wang, L. Yolk-Shell Nanostructured Fe_3O_4@C Magnetic Nanoparticles with Enhanced Peroxidase-Like Activity for Label-Free Colorimetric Detection of H_2O_2 and Glucose. *Nanoscale* **2017**, *9*, 4508−4515.
(40) Liu, B.; Liu, J. Accelerating Peroxidase Mimicking Nanozymes Using DNA. *Nanoscale* **2015**, *7*, 13831−13835.
(41) Farka, Z.; Čunderlová, V.; Horáčková, V.; Pastucha, M.; Mikušová, Z.; Hlaváček, A.; Skládal, P. Prussian Blue Nanoparticles as a Catalytic Label in a Sandwich Nanozyme-Linked Immunosorbent Assay. *Anal. Chem.* **2018**, *90*, 2348−2354.
(42) Zhang, R.; Lu, N.; Zhang, J.; Yan, R.; Li, J.; Wang, L.; Wang, N.; Lv, M.; Zhang, M. Ultrasensitive Aptamer-Based Protein Assays Based on One-Dimensional Core-Shell Nanozymes. *Biosens. Bioelectron.* **2020**, *150*, 111881.
(43) Zhang, L.; Qi, Z.; Zou, Y.; Zhang, J.; Xia, W.; Zhang, R.; He, Z.; Cai, X.; Lin, Y.; Duan, S.-Z.; Li, J.; Wang, L.; Lu, N.; Tang, Z. Engineering DNA-Nanozyme Interfaces for Rapid Detection of Dental Bacteria. *ACS Appl. Mater. Interfaces* **2019**, *11*, 30640−30647.
(44) Albanese, A.; Chan, W. C. W. Effect of Gold Nanoparticle Aggregation on Cell Uptake and Toxicity. *ACS Nano* **2011**, *5*, 5478−5489.
(45) Patil, A. J.; Vickery, J. L.; Scott, T. B.; Mann, S. Aqueous Stabilization and Self-Assembly of Graphene Sheets into Layered Bio-Nanocomposites using DNA. *Adv. Mater.* **2009**, *21*, 3159−3164.
(46) Li, Q.; Lu, N.; Wang, L.; Fan, C. Advances in Nanowire Transistor-Based Biosensors. *Small Methods* **2018**, *2*, 1700263.
(47) Gao, A.; Lu, N.; Dai, P.; Li, T.; Pei, H.; Gao, X.; Gong, Y.; Wang, Y.; Fan, C. Silicon-Nanowire-Based CMOS-Compatible Field-Effect Transistor Nanosensors for Ultrasensitive Electrical Detection of Nucleic Acids. *Nano Lett.* **2011**, *11*, 3974−3978.
(48) Zhang, M.; Zheng, J.; Wang, J.; Xu, J.; Hayat, T.; Alharbi, N. S. Direct Electrochemistry of Cytochrome c Immobilized on One Dimensional Au Nanoparticles Functionalized Magnetic N-Doped Carbon Nanotubes and Its Application for the Detection of H_2O_{2r}. *Sensor. Actuator. B Chem.* **2019**, *282*, 85−95.
(49) Lu, N.; Gao, A.; Dai, P.; Song, S.; Fan, C.; Wang, Y.; Li, T. CMOS-Compatible Silicon Nanowire Field-Effect Transistors for Ultrasensitive and Label-Free MicroRNAs Sensing. *Small* **2014**, *10*, 2022−2028.

https://dx.doi.org/10.1021/acsabm.0c00588
ACS Appl. Bio Mater. 2020, 3, 5111−5119

(50) Kumar, S.; Rani, R.; Dilbaghi, N.; Tankeshwar, K.; Kim, K.-H. Carbon Nanotubes: A Novel Material for Multifaceted Applications in Human Healthcare. *Chem. Soc. Rev.* **2017**, *46*, 158−196.
(51) Han, F.; Ma, L.; Sun, Q.; Lei, C.; Lu, A. Rationally Designed Carbon-Coated Fe_3O_4 Coaxial Nanotubes with Hierarchical Porosity as High-Rate Anodes for Lithium Ion Batteries. *Nano Res.* **2014**, *7*, 1706−1717.
(52) Wei, W.; Yang, S.; Zhou, H.; Lieberwirth, I.; Feng, X.; Müllen, K. 3D Graphene Foams Cross-linked with Pre-encapsulated Fe_3O_4 Nanospheres for Enhanced Lithium Storage. *Adv. Mater.* **2013**, *25*, 2909−2914.
(53) Salimian, M.; Ivanov, M.; Deepak, F. L.; Petrovykh, D. Y.; Bdikin, I.; Ferro, M.; Kholkin, A.; Titus, E.; Goncalves, G. Synthesis and Characterization of Reduced Graphene Oxide/Spiky Nickel Nanocomposite for Nanoelectronic Applications. *J. Mater. Chem. C* **2015**, *3*, 11516−11523.
(54) Mao, Y.; Duan, H.; Xu, B.; Zhang, L.; Hu, Y.; Zhao, C.; Wang, Z.; Chen, L.; Yang, Y. Lithium Storage in Nitrogen-Rich Mesoporous Carbon Materials. *Energy Environ. Sci.* **2012**, *5*, 7950−7955.
(55) Wang, X.; Cao, W.; Qin, L.; Lin, T.; Chen, W.; Lin, S.; Yao, J.; Zhao, X.; Zhou, M.; Hang, C.; Wei, H. Boosting the Peroxidase-Like Activity of Nanostructured Nickel by Inducing Its 3+ Oxidation State in $LaNiO_3$ Perovskite and Its Application for Biomedical Assays. *Theranostics* **2017**, *7*, 2277−2286.
(56) Yu, J.; Ma, T.; Liu, S. Enhanced Photocatalytic Activity of Mesoporous TiO_2 Aggregates by Embedding Carbon Nanotubes as Electron-Transfer Channel. *Phys. Chem. Chem. Phys.* **2011**, *13*, 3491−3501.
(57) Wei, H.; Wang, E. Fe_3O_4 Magnetic Nanoparticles as Peroxidase Mimetics and Their Applications in H_2O_2 and Glucose Detection. *Anal. Chem.* **2008**, *80*, 2250−2254.
(58) Guo, Z.; Xu, J.; Zhang, J.; Hu, Y.; Pan, Y.; Miao, P. A Facile Strategy for Electrochemical Analysis of Hydrogen Peroxide Based on Multifunctional Fe3O4@Ag Nanocomposites. *ACS Appl. Bio Mater.* **2018**, *1*, 367−373.
(59) Ding, Y.; Yang, B.; Liu, H.; Liu, Z.; Zhang, X.; Zheng, X.; Liu, Q. FePt-Au Ternary Metallic Nanoparticles with the Enhanced Peroxidase-Like Activity for Ultrafast Colorimetric Detection of H_2O_2. *Sensor. Actuator. B Chem.* **2018**, *259*, 775−783.
(60) Sheng, Z. M.; Gan, Z. Z.; Huang, H.; Niu, R. L.; Han, Z. W.; Jia, R. P. M-N_x (M = Fe, Co, Ni, Cu) Doped Graphitic Nanocages with High Specific Surface Area for Non-enzymatic Electrochemical Eetection of H_2O_2. *Sensor. Actuator. B Chem.* **2020**, *305*, 127550.
(61) Xu, S.; Wang, Y.; Zhou, D.; Kuang, M.; Fang, D.; Yang, W.; Wei, S.; Ma, L. A Novel Chemiluminescence Sensor for Sensitive Detection of Cholesterol Based on the Peroxidase-Like Activity of Copper Nanoclusters. *Sci. Rep.* **2016**, *6*, 39157.
(62) Zhang, Y.; Wang, Y.-N.; Sun, X.-T.; Chen, L.; Xu, Z.-R. Boron Nitride Nanosheet/CuS Nanocomposites as Mimetic Peroxidase for Sensitive Colorimetric Detection of Cholesterol. *Sensor. Actuator. B Chem.* **2017**, *246*, 118−126.
(63) Li, Y.; Kang, Z.; Kong, L.; Shi, H.; Zhang, Y.; Cui, M.; Yang, D.-P. MXene-Ti_3C_2/CuS Nanocomposites: Enhanced Peroxidase-Like Activity and Sensitive Colorimetric Cholesterol Detection. *Mater. Sci. Eng., C* **2019**, *104*, 110000.
(64) Zhao, L.; Wu, Z.; Liu, G.; Lu, H.; Gao, Y.; Liu, F.; Wang, C.; Cui, J.; Lu, G. High-Activity Mo, S co-Doped Carbon Quantum Dot Nanozyme-Based Cascade Colorimetric Biosensor for Sensitive Detection of Cholesterol. *J. Mater. Chem. B* **2019**, *7*, 7042−7051.

https://dx.doi.org/10.1021/acsabm.0c00588
ACS Appl. Bio Mater. 2020, 3, 5111−5119